Unsteady Aerodynamic and Optimal Kinematic Analysis of a Micro Flapping Wing Rotor

H Li[1], S Guo[1,*], Y L Zhang[2], C Zhou[2] and J H Wu[2]
[1]Centre for Aeronautics, SATM, Cranfield University, Cranfield, Beds, UK
[2]School of Transport Science and Engineering, Beihang University, Beijing, China

E-mail: s.guo@cranfield.ac.uk

Abstract. Inspired by the high performance of rotary and insect flapping wings capable of vertical take-off and landing and hovering (VTOLH), a novel flapping wing rotor (FWR) has been developed by combining the above two types of wing motions. The FWR offers an alternative configuration for micro air vehicles (MAV) of such high flight performance. Unlike the well-studied aerodynamics of rotary and insect-like flapping wing with prescribed wing motion, the aerodynamic lift and efficiency of the FWR associated with optimal kinematics of motion has not been studied in a systematic manner before. This investigation is therefore focused on the FWR optimal kinematic motion in terms of aerodynamic lift and efficiency. Aerodynamic analysis is conducted for a FWR model of aspect ratio 3.6 and wing span 200mm in a range of kinematic parameters. The analysis is based on a quasi-steady aerodynamic model with empirical coefficients and validated by CFD results at Re~3500. For comparison purpose, the analysis includes rotary and insect-like flapping wings in hovering status with the FWR at an equilibrium rotation speed when the thrust equals to drag. The results show that the rotary wing has the greatest power efficiency but the smallest lift coefficient. Whereas the FWR can produce the greatest aerodynamic lift with power efficiency between rotary and insect-like flapping wings. The results provide a quantified guidance for design option of the three types of high performance MAVs together with the optimal kinematics of motion according to flight performance requirement.

Keywords: Bioinspired FWR, MAV, flapping wing, optimal kinematics, aerodynamic efficiency.

1. Introduction

Micro air vehicles (MAV) with small dimension and low flight speed (Reynolds number: $Re \sim 10^3$) are of special interest for both military and civil applications. The standard layouts of existing MAVs include the well-studied fixed wing and rotary wing of conventional aircrafts and the flapping wing inspired by insects and birds [1]. Despite the various existing layouts, the aerodynamic performance of MAVs in low Re flight is still a major limitation for a practical design, especially in terms of the lift production and power efficiency. In order to extend the current limitations, a novel concept of flapping wing rotor (FWR) which combines both the insect flapping wing and man-made rotary wing has been proposed by the authors [2]. Like the insect wing and rotary wing, the FWR makes use of gyration of the wing with respect to the root to produce a velocity relative to the surrounding air. On the other

---

hand, the FWR wing combines an active vertical flapping and a passive horizontal rotation, which leads to a self-balanced equilibrium motion in the horizontal plane, with no reaction torque exerting on the body, as opposed to the conventional rotorcraft. This leads to a potential power saving and system simplicity. Thus, the novel concept of FWR may be suited for developing MAVs with vertical take-off and landing and hovering (VTOLH) capability and operate in complex and risky environments and inside buildings [2].

For rotary wing and insect flapping wing, the aerodynamic performances at low Re ($\sim10^3$) have been studied extensively by previous authors [3–7]. Several unsteady aerodynamic mechanisms are found to enhance lift for insect wings. In particular, the stable leading edge vortex (LEV) provides the majority of lift enhancement (about 80% for angles of attack above 13.5˚, [8]), while rotational circulation and added mass effects contribute to the instantaneous peaks at stroke reversals [4]. The stability of LEV is crucial for the high lift production of insect wings, and has been addressed with particular attention. Ellington et al [5] suggested that the spanwise velocity along the LEV core serves to transport vorticity towards wingtip, which stabilizes LEV in a similar manner with conventional delta wings. Lim et al [9] with experimental and numerical approach showed that the vortex stretching could significantly delay the detachment of the LEV, even when the spanwise flow was weak. In an experimental study of unidirectional rotating wing, Lentink and Dickinson [10] found that LEV could be stabilized by the centripetal and Coriolis accelerations at low Rossby number (Ro, see definition in section 2.2), and this effect appears to be independent of Re in a wide range (Re=100~14000).

While the rotary wing and insect flapping wing with their prescribed motions have been studied on extensively, the FWR wing aerodynamic behaviours for MAV design has received less study. Wu et al [11] used a CFD method to analysis the forces production of FWR at Re =350~9000. Their results showed that the LEV formed on the wing of FWR stays attached throughout the flapping cycle, which provides lift enhancement similar to insect wings. Zhou et al and Guo et al [12,13] in experimental and numerical studies found that the aerodynamic performance of FWR varies critically with the pitching kinematics of wing motion. By effectively changing the pitch angles in the upstroke and downstroke, the FWR will achieve different status for lift and efficiency. Previous experimental studies showed that a rotary wing at low Ro was able to sustain attached LEV [10,14,15]. Furthermore, Lentink and Dickinson [10] showed that the rotary wing exhibits higher aerodynamic efficiency than insect wings for hovering in a wide range of Re (Re=100~14000). Lentink et al [16] further argued that the rotary wing may be the most energy efficient layout for insect-sized MAVs. Despite these new findings, a practical MAV design is still challenged by the efficiency and lift requirements associated with the low Re flight. Kinematic strategies to explore the optimal performances could provide significant guidance for MAV design in a practical scenario. Therefore, the current study is focused on investigating the optimal kinematics for lift and efficiency of the FWR wing, and compare with the conventional rotary wing and insect flapping wing motions.

Experimental and numerical studies showed that the aerodynamic force on a wing operating reciprocal flapping and pitching motion could be modelled by a quasi-steady aerodynamic theory [15,17–19]. In the current study, a quasi-steady aerodynamic model for the FWR has been built and validated in a range of kinematic parameters. In addition to the LEV, the rotational circulation and the added mass inertia were taken into account for aerodynamic force modelling. Based on the equilibrium status of FWR, the effect of pitch angles and non-dimensional rotation speed for lift production and efficiency are analysed. The optimal kinematics of FWR for both lift and efficiency have been determined. Further, the aerodynamic performances of FWR are compared with the other two competitive wings for MAVs, i.e. the insect flapping wing and rotary wing (RW) capable of VTOLH. For the insect flapping wings, comparisons are made with two types of kinematics namely the horizontal flapping (HF) and inclined flapping (IF) demonstrated typically by fruitfly and dragonfly respectively.

In this investigation, a wing model of aspect ratio (AR) 3.6 and 200mm span is taken as example for analysis at Re~3500 (see definition in section 2.2). The kinematics for both FWR and insect wings are set in a simple harmonic motion. To determine the optimal kinematics for FWR, the pitch angle of the wing varies in the range of <90$^\text{o}$. The wing flaps between the angle of ±25$^\text{o}$ and at frequency ~12Hz.

The aerodynamic lift and efficiency at the same *Re* for insect wing and rotary wing are obtained at specified parameter range chosen from typical insect data. The results show that the rotary wing has the greatest power efficiency but smallest lift coefficient. While the FWR can produce the greatest aerodynamic lift with a power efficiency standing between the other two types. The study provides a basis for insight into the kinematics strategy and unsteady aerodynamics in low *Re* flight. From the results, an MAV design choice from the three types of wings associated with their optimal kinematics can be made for either a maximum lift with a specified efficiency or a maximum efficiency with a required lift.

2. FWR model and analysis method

2.1. FWR coordinate and kinematics

The coordinate systems used to describe the FWR kinematics of motion are shown in figure 1(a). The FWR body is depicted in the figure with the wing detached for clarity. The coordinate systems include the inertial frame (x, y, z), the wing-fixed frame (x_w, y_w, z_w), and the intermediate frame of the *Euler* rotations (x', y', z') and (x'', y'', z''). For clarity, the overlapping axes of the intermediate frames x', y'' and z'' are omitted. The inertial frame (x, y, z) is attached to the body with the origin 'o' at the wing root; the wing-fixed frame (x_w, y_w, z_w) is attached to the wing root with the same origin. The rotation plane is set in horizontal. The FWR rotation, flapping, and pitching angles are given by ψ, ϕ and α, respectively. The wing motion is described by successive rotation about the y, x' and z_w axis with the corresponding *Euler* angles (positive anticlockwise). The planar views with respect to each axis describing the corresponding *Euler* angles are shown in figure 1(b).
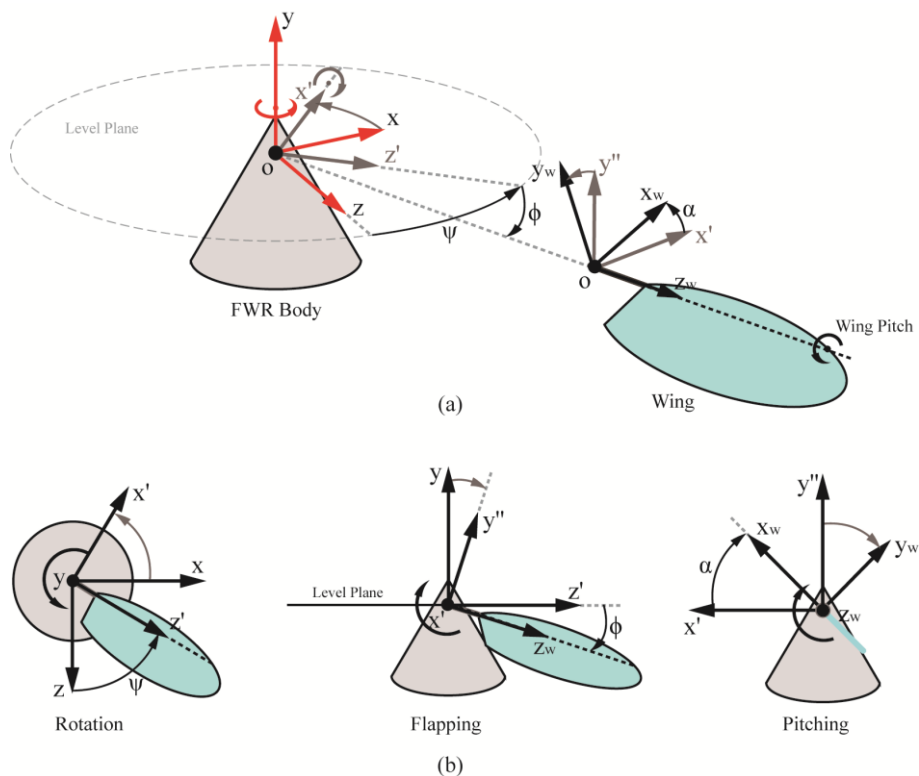
Figure 1. (a) Coordinate systems and rotation angles definitions for the FWR wing. (b) The top, back and side view of the *Euler* angles.

3

Based on the above definition, the angular velocity vector of the FWR wing in the inertial frame can be expressed by the time derivative of the three *Euler* angles $\dot{\psi}$, $\dot{\phi}$, and $\dot{\alpha}$ and the transformation matrixes:

$$\vec{\omega}_i = \begin{bmatrix} \omega_i & \omega_j & \omega_k \end{bmatrix}^T = \begin{bmatrix} 0 \\ \dot{\psi} \\ 0 \end{bmatrix} + \mathbf{R}(\psi) \begin{bmatrix} \dot{\phi} \\ 0 \\ 0 \end{bmatrix} + \mathbf{R}(\psi)\mathbf{R}(\phi) \begin{bmatrix} 0 \\ 0 \\ \dot{\alpha} \end{bmatrix} \tag{1}$$

where $\mathbf{R}(\psi)$ and $\mathbf{R}(\phi)$ are the rotation matrixes of the corresponding *Euler* angles; $[\cdot]^T$ indicates matrix transpose. The angular acceleration vector in the inertial frame $\dot{\vec{\omega}}_i$ can be derived by directly differentiating the above equation. By combining the three elementary rotations, the transformation matrix from inertial frame to the wing-fixed frame is given as:

$$\mathbf{R}_{i \to w} = \mathbf{R}^T(\alpha)\mathbf{R}^T(\phi)\mathbf{R}^T(\psi) \tag{2}$$

The angular velocity and acceleration vector in the wing-fixed frame is obtained by applying the above transformation. For blade element analysis, it is convenient to write down the velocity and acceleration of a 2D wing chord due to the gyration of the wing at span-wise location r. The resultant velocity and acceleration vector when expressed in the wing-fixed frame are planar vectors with only two nontrivial indices, i.e. the x_w and y_w components:

$$\vec{U}(r) = \vec{\omega} \times \vec{r} = \omega_y r \mathbf{e_x} - \omega_x r \mathbf{e_y} = \begin{bmatrix} u_x & u_y & 0 \end{bmatrix}^T \tag{3a}$$

$$\dot{\vec{U}}(r) = \dot{\vec{\omega}} \times \vec{r} + \vec{\omega} \times (\vec{\omega} \times \vec{r}) = (\dot{\omega}_y + \omega_x\omega_z)r\mathbf{e_x} + (-\dot{\omega}_x + \omega_y\omega_z)r\mathbf{e_y} = \begin{bmatrix} \dot{u}_x & \dot{u}_y & 0 \end{bmatrix}^T \tag{3b}$$

where $\mathbf{e_x}$, $\mathbf{e_y}$ represent the basis vector of the wing-fixed coordinate system of the 2D wing section; $\vec{\omega}$ denote the rotation rate of the wing in the wing-fixed coordinate system, which has ω_x, ω_y and ω_z components in the x_w, y_w and z_w axes, respectively; $\vec{U}(r)$ and $\dot{\vec{U}}(r)$ refers to the velocity and acceleration vector of the 2D wing chord at span-wise location r; u_x, u_y, $\dot{u}_x$ and $\dot{u}_y$ are used to represent the components of velocity and acceleration in x_w and y_w axes, respectively. Based on these kinematic parameters, the effective angle of attack (AoA) of the wing at any instantaneous time can be determined by inversing the trigonometric function of the velocity ratio:

$$\alpha_e = \arctan\left(\frac{u_y}{u_x}\right) \tag{4}$$

The key feature of the FWR kinematics is the coupled flapping and rotation motion and asymmetric pitching at up and downstroke, as shown in figure 2. In these degrees of freedom, the definition of a specific function to describe the wing motion varies. However, major properties of the aerodynamic performance can be seized by simple harmonic motion [20]. In the current study, the FWR is set in a sinusoidal flapping while rotate at a constant speed ($\dot{\psi} = \psi_0$). The flapping velocity of the wing is given by the function:

$$\dot{\phi} = \pi f \Phi \cos\left(2\pi\hat{t} + \frac{\pi}{2}\right) \tag{5a}$$

where f is the flapping frequency, Φ is the flapping amplitude, $\hat{t} = ft$ is the non-dimensional time. The pitching velocity of the wing is set plateaued in the mid-strokes by modifying the sinusoidal function:

$$\dot{\alpha} = 2f(\alpha_u - \alpha_d)\{(-1)^{[2\hat{t}+0.5]} - \cos(4\pi\hat{t} + [2\hat{t} - 0.5]\pi)\} \tag{5b}$$

where α_u and α_d are the geometric AoA of the wing at mid-upstroke and mid-downstroke. The bracket notation $[\cdot]$ is understood as the floor function giving the greatest bounding integer.

The resulting kinematics of the wing defined as above is illustrated in figure 2. The tip trajectory of the wing shows a coupled flapping and rotation motion. Similar to a dragonfly wing, the pitching is asymmetric with different α_u and α_d at up and downstrokes, respectively.
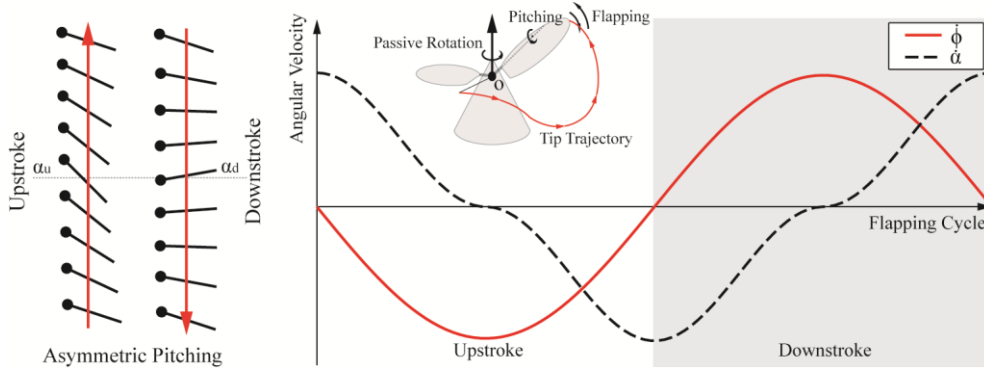
Figure 2. The kinematic pattern of the FWR wing.

2.2. The FWR wing geometry

The FWR wing used in the current investigation is a thin flat plate of elliptical shape as shown in figure 3. The wing has chord-wise cutting edge near the root. The non-dimensional radius of the first, second and third area moments $\hat{R}_1$, $\hat{R}_2$ and $\hat{R}_3$ of the wing are defined by:

$$\hat{R}_k = \sqrt[k]{\frac{AR \int_0^R c(r)r^k dr}{R^{k+2}}}, \ k = 1, 2, 3 \tag{6}$$

where $c(r)$ is the local chord length, R is the wing semi-span, AR=3.6 is the aspect ratio. These are the shape parameters for the wing geometry. In order to keep the morphological similarity with insect wings, the parameters $\hat{R}_1$, $\hat{R}_2$ and $\hat{R}_3$ are constrained by the numbers 0.45~0.55, 0.5~0.6 and 0.55~0.65, respectively [21]. In addition, the Ro is defined by [10]:

$$Ro = \frac{R_2}{\bar{c}} \tag{7}$$

where $R_2 = \hat{R}_2 R$ is the radius of the second area moment, and $\bar{c} = \frac{R}{AR}$ is the mean chord length. For hovering flight, Ro is equivalent to AR and is given by the value Ro=2.1 in the current study. The geometric parameters of the FWR wing are listed below:

$$AR = 3.6, \ Ro = 2.1, \ \hat{R}_1 = 0.55, \ \hat{R}_2 = 0.59, \ \hat{R}_3 = 0.63 \tag{8}$$
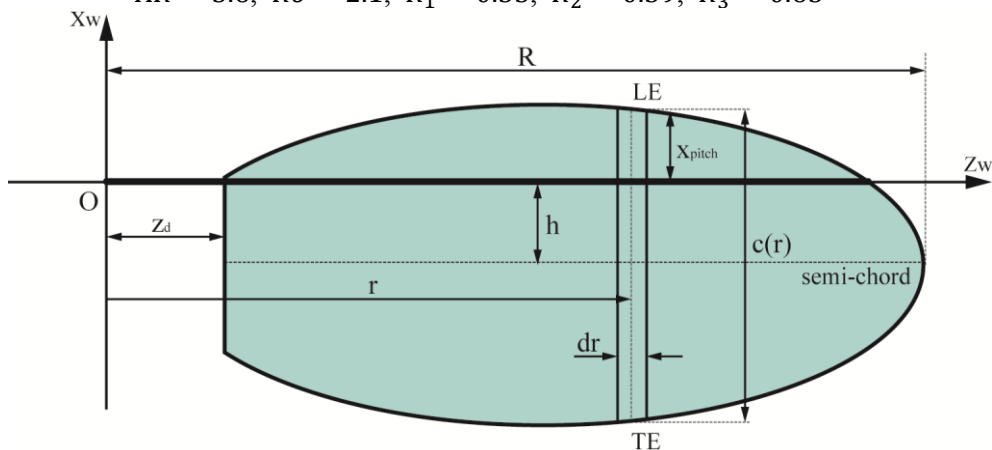
Figure 3. Wing geometric definitions in the wing-fixed coordinate system.

The wing surface starts with a distance z_d from the wing root. At span-wise location r, a wing strip of width dr and chord length $c(r)$ is shown in the figure; h is the vertical coordinate of the semi-chord of

5

the ellipse. The z_w axis of the wing is located in a distance x_{pitch} from the leading edge (LE), which can be expressed as:

$$x_{pitch} = \left(\frac{1}{2} + \hat{h}\right) c(r) \tag{9}$$

where $\hat{h}$ is the non-dimensional local coordinate of the semi-chord: $\hat{h} = \frac{h}{c(r)}$. For insect flapping wing, the pitching axis (z_w) is usually considered to locate at around 0.25 chord length [18,22], corresponding to $\hat{h} = -0.25$. This value is used in the current model for calculation.

The Reynolds number in the current investigation is defined by:

$$Re = \frac{2\Phi f R \bar{c}}{\nu} \tag{10}$$

where Φ and f are the flapping amplitude and frequency, ν is the kinematic viscosity. For our specified Re (~ 3500), the wing semi-span is fixed by the value of $R = 100$ mm while the flapping frequency and amplitude varies accordingly in different kinematic cases.

2.3. FWR aerodynamic model

Like the insect wing, the unsteady aerodynamic force of FWR is generated by active flapping and pitching motion. Unlike the insect wing, the FWR produces an additional self-propelled rotation. The quasi-steady aerodynamic model for predicting the aerodynamic forces of insect flapping wings [4,19,23] is adapted in the current study for FWR. In this model, the aerodynamic force coefficients are updated by an empirical fit of data that include the unsteady effects of the flow. For a 2D spanwise strip, the model is expressed in the form with instantaneous force depend only upon the status, velocity and acceleration of the wing:

$$dF_x(r) = \left\{\frac{1}{2}\rho|\vec{U}(r)|^2 C_H(\alpha_e)c(r) + \left(\lambda_y u_y \omega_z - \lambda_{y\omega}\omega_z^2\right)\right\} dr \tag{11a}$$

$$dF_y(r) = \left\{\frac{1}{2}\rho|\vec{U}(r)|^2 C_V(\alpha_e)c(r) + C_{rot}\rho|\vec{U}(r)|\omega_z c(r)^2 + \left(-\lambda_y \dot{u}_y + \lambda_{y\omega}\dot{\omega}_z\right)\right\} dr \tag{11b}$$

where $|\cdot|$ indicates the *Euclidean* norm; ρ is the air density; α_e is effective AoA of the wing obtained by equation (4); $c(r)$ is the local chord length; $C_V(\alpha_e)$ and $C_H(\alpha_e)$ are the 'steady' force coefficients due to wing translation; C_{rot} is the rotational force coefficient due to wing pitching; λ_y and $\lambda_{y\omega}$ are the added mass coefficients.

In the above equations, the forces and kinematic parameters are expressed in the wing-fixed frame (x_w, y_w, z_w) (see (3a)$\sim$(3b) for the definitions of kinematic parameters). Equation (11a) accounts for the force parallel to the wing chord with the steady term and the added mass term [17,24]. The added mass coefficients λ_y and $\lambda_{y\omega}$ for a 2D flat plate moving in potential flow are given by $\lambda_y = \frac{\pi}{4}\rho c(r)^2$, $\lambda_{y\omega} = \frac{\pi}{4}\rho\hat{h}c(r)^3$. Equation (11b) accounts for the force acting perpendicular to the wing chord, with the steady force as the first term, the wing rotation force as the second term and the added mass force as the third term.

The translational force coefficients on a 2D wing section are illustrated in figure 4. Empirical fit of experimental data shows that the coefficients in the aerodynamic frame $\vec{C}_F = [C_d, C_l]^T$ obey the following trigonometric relation [19,23]:

$$\begin{cases} C_l = C_{Lmax}\sin(2\alpha_e) \\ C_d = \left(\frac{C_{Dmax}+C_{D0}}{2}\right) - \left(\frac{C_{Dmax}-C_{D0}}{2}\right)\cos(2\alpha_e) \end{cases} \tag{12}$$

For a particular wing geometry and Re, the constants C_{Lmax}, C_{Dmax}, C_{D0} together with C_{rot} can be obtained by empirical fit of experimental data. Sane and Dickinson [17,18] used a model fruitfly (*Drosophila melanogaster*) wing to obtain the coefficients at $Re\sim100$. When the pitching axis of the wing was located at 0.25 chord distance, the above coefficients were given by $C_{Lmax} = 1.8$, $C_{Dmax} = 3.4$ and $C_{D0} = 0.4$. While C_{rot} was between 0.5$\sim$1.8, which depends on the pitching rate of the wing.

In an further study, Lee *et al* [25] adapted the quasi-steady model to account for the effect of Ro, AR and taper ratio of the wing, thus extended the applicability of the model to a wider range of flow conditions and wing geometry. For the purpose of the current study, an empirical fit of the quasi-steady coefficients have been used in our model. The aerodynamic data was obtained by using the CFD method for the particular wing geometry (see figure 3), Ro (=2.1) and Re (~3500). The quasi-steady coefficients by fitting the CFD data are given by $C_{Lmax} = 1.7$, $C_{Dmax} = 3.24$ and $C_{D0} = 0.05$. Whereas for our current investigation with moderate wing pitching rate, C_{rot} has been taken as $C_{rot}=1.0$ in our model.
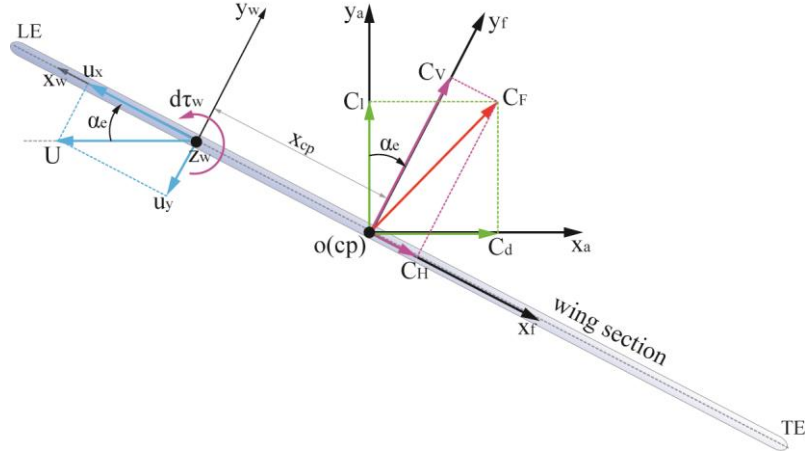
Figure 4. Coordinate systems, velocity and forces vectors on a 2D wing section ('o' indicates the centre of pressure).

Based on equation (12), the translational force coefficients $\vec{C}_F = [C_H \ C_V]^T$ are obtained by frame transformation:

$$\begin{bmatrix} C_H \\ C_V \end{bmatrix} = R(\alpha_e) \begin{bmatrix} C_d \\ C_l \end{bmatrix} \tag{13}$$

where the transformation matrix $\mathbf{R}(\alpha_e)$ is from the aerodynamic frame (x_a, y_a) to the wing-fixed frame (x_w, y_w).

The aerodynamic torque $d\tau_w$ (pitch moment about z_w axis) of the 2D wing section is obtained by the summing the translational torque $d\tau_{qs}$, the aerodynamic damping torque $d\tau_{rd}$ [23,26] and the torque $d\tau_{am}$ due to added mass force:

$$d\tau_w(r) = d\tau_{qs} + d\tau_{rd} + d\tau_{am} \tag{14}$$

Each of these terms is calculated by the following equations:

$$d\tau_{qs} = -\frac{1}{2}\rho\left|\vec{U}(r)\right|^2 C_V(\alpha_e)\hat{x}_{cp}c^2(r)dr \tag{15a}$$

$$d\tau_{rd} = -\frac{1}{2}\rho\omega_z|\omega_z|C_{rd}\hat{x}_{rd}c^4(r)dr \tag{15b}$$

$$d\tau_{am} = \left[\lambda_y u_x u_y - \lambda_{y\omega}(\dot{u}_y + u_x\omega_z) + \lambda_\omega\dot{\omega}_z\right]dr \tag{15c}$$

where C_{rd} is the rotational damping torque coefficient; $\hat{x}_{cp}$ is the non-dimensional chord-wise centre of pressure (CP) of the translational force; $\hat{x}_{rd}$ is the non-dimensional location of the rotational damping force; λ_ω is added mass torque coefficient, and is given as: $\lambda_\omega = \left[\frac{\pi}{4}\rho\hat{h}^2 + \frac{\pi}{128}\rho\right]c(r)^4$ [24].

For insect-like flapping wings, $\hat{x}_{cp}$ varies linearly with the effective AoA α_e, and is obtained empirically by [27]:

$$\hat{x}_{cp} = \frac{0.82}{\pi}|\alpha_e| - \hat{h} - 0.45 \tag{16}$$

The non-dimensional location of rotational damping force $\hat{x}_{rd}$ is given by [23,26]:

$$\hat{x}_{rd} = \frac{1}{2}\hat{h}^4 + \frac{3}{4}\hat{h}^2 + \frac{1}{32} \tag{17}$$

Andersen *et al* [26] used a rotational damping torque coefficient of $C_{rd} = 2.0$ for predicting the unsteady aerodynamic force of tumbling cards. Based on experimental study of insect wing, Whitney and Wood [23] proposed the coefficient C_{rd} equal to the maximum drag coefficient C_{Dmax} since the rotationally induced velocity is normal to the wing. This assumption is used in our current model.

Based on the 2D aerodynamic forces and torques described above, the 3D force $\vec{F}_w = \begin{bmatrix} F_x & F_y & 0 \end{bmatrix}^T$ and torque $\vec{\tau}_w = \begin{bmatrix} \tau_x & \tau_y & \tau_z \end{bmatrix}^T$ of the wing can be obtained by integrating the elementary forces and torques along the span R:

$$\begin{cases} F_{x;y} = \int_{r=0}^{R} dF_{x;y}(r) \\ \tau_x = -\int_{r=0}^{R} r dF_y(r) \\ \tau_y = \int_{r=0}^{R} r dF_x(r) \\ \tau_z = \int_{r=0}^{R} d\tau_w(r) \end{cases} \tag{18}$$

2.4. Power consumption

For a real FWR wing, the majority of power consumption would come from the power to accelerate the wing inertia and the power to overcome the aerodynamic drag. For insect flight, mechanical power can be stored in elastic structure (such as the thorax), and released in the subsequent flapping stroke [28]. Previous studies showed that for the insect flapping kinematics, the interplay between the wing inertia and aerodynamic force has strong implications on the power consumptions [29]. In particular, the passive pitching of flapping wing by its own inertia may help to overcome the aerodynamic torque which saves energy for insect flight.

In the current study, we focus on the aerodynamic power of FWR in hovering. The instantaneous power is thus obtained directly by the inner product of the angular velocity $\vec{\omega}$ with the aerodynamic torque $\vec{\tau}_w$:

$$P_{aero} = -\vec{\omega} \cdot \vec{\tau}_w \tag{19}$$

where positive value indicates power consumption and negative value indicates power input to the system. The time averaged energy cost of the FWR wing over a flapping cycle can be obtained by:

$$\bar{P} = \frac{1}{T} \int_{t=0}^{T} P_{aero} dt \tag{20}$$

where T is the flapping period.

3. Quasi-steady model validation and discussion

To validate the aerodynamic model, the aerodynamic lift and rotational moment of FWR at $Re \sim 10^3$ are compared with the results from CFD method. In this calculation, the FWR wing used the same geometry and kinematic parameters as given in the CFD analysis [11]. The lift and rotational moment coefficients are defined by:

$$C_L = \frac{L}{0.5\rho U_{ref}^2 S} \tag{21a}$$

$$C_M = \frac{M}{0.5\rho U_{ref}^2 S \bar{c}} \tag{21b}$$

where $U_{ref} = 2\Phi f R_2$ is the mean flapping velocity at the radius of second area moment [30], L is the instantaneous lift and M is the instantaneous rotational moment, S is the wing area. Similarly, the time averaged values of the above coefficients $\bar{C}_L$ and $\bar{C}_M$ are obtained by using the mean lift force

$\bar{L} = \frac{\int_0^T L dt}{T}$ and mean rotational moment $\bar{M} = \frac{\int_0^T M dt}{T}$ instead of the instantaneous values (L and M) in the above equations.

We chose different kinematic cases varying the flapping amplitude Φ, the geometric AoAs (α_u and α_d), and the periodic ratio of flapping to rotation n (defined as the ratio of flapping period T_f to rotation period T_r: $n = \frac{T_f}{T_r}$, [11]) for comparison. The kinematic parameters and the resulting mean lift and rotational moment coefficients are presented in Table 1. Figure 5 shows the comparison of instantaneous lift and rotational moment coefficients (C_L and C_M).
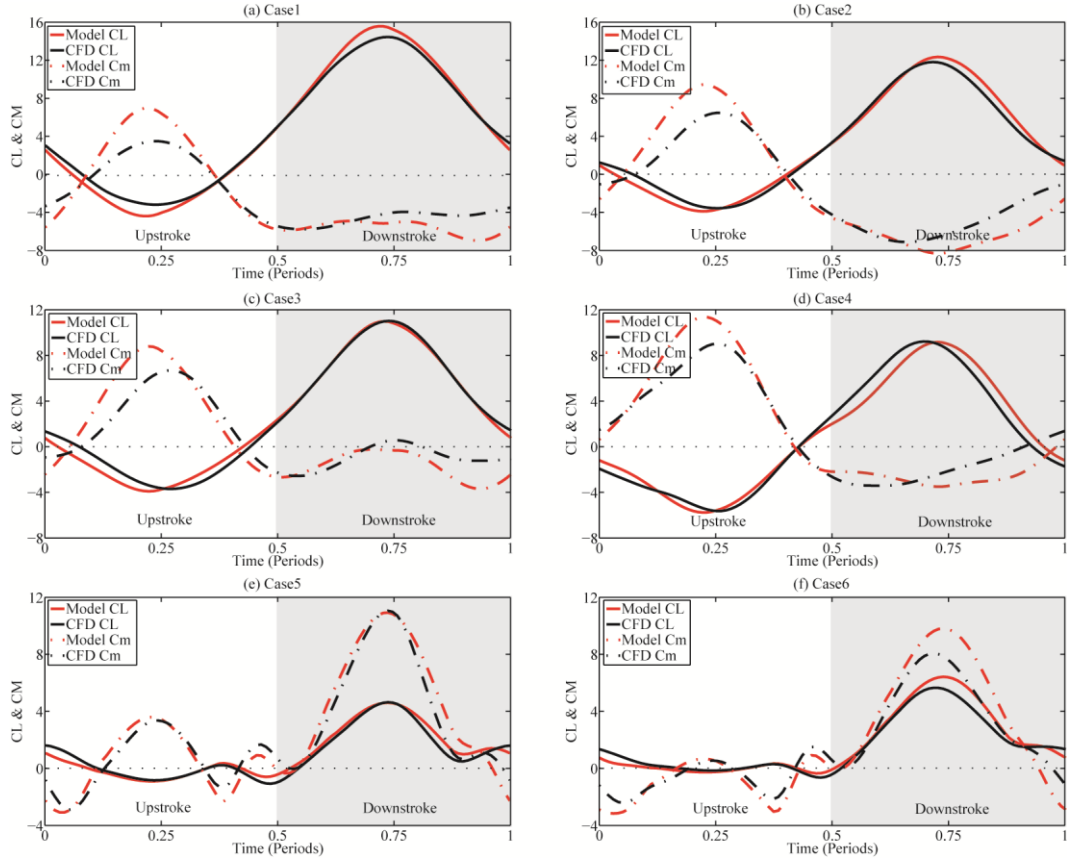
Figure 5. Lift and rotational moment coefficients (C_L and C_M) comparisons of the quasi-steady model and CFD method.

Table 1. Time averaged coefficients ($\bar{C}_L$, $\bar{C}_M$) by quasi-steady model and CFD method.

Kinematic Parameters				CFD Results		Quasi-steady Results	
Case No.	Φ	n	α_u	α_d	$\bar{C}_L$	$\bar{C}_M$	$\bar{C}_L$	$\bar{C}_M$
1	20°	0.25	25°	5°	5.11	-2.38	5.06 (-1.0%)	-2.42 (1.6%)
2	30°	0.25	30°	10°	3.27	-1.57	3.32 (1.4%)	-1.69 (7.4%)
3	30°	0.25	30°	0°	2.81	0.77	2.68 (-4.6%)	0.76 (-2.1%)
4	30°	0.13	25°	5°	1.00	1.33	1.08 (8.6%)	1.42 (6.2%)
5	70°	0.42	50°	-30°	0.92	2.39	1.02 (11.7%)	2.55 (6.8%)
6	70°	0.33	60°	-20°	1.55	1.53	1.70 (9.5%)	1.75 (15%)

For the FWR wing, the applicability of the quasi-steady model relies essentially on the stability of LEV. This flow structure has been observed on insect wings by both experimental and numerical methods. By observing the flow structure of a hawkmoth (*Manduca sexta*) wing in a typical motion, Ellington *et al* [5] found a strong spanwise flow along the LEV core. Based on this observation, they proposed that LEV could be stabilized by the spanwise flow which transports vorticity of the LEV towards wingtip, thus delays the shedding of LEV. Lim *et al* [9] through experimental and numerical methods found that the LEV could be stabilized due to vortex stretching even with a weak spanwise flow. By examining the LEV dynamics of unidirectional rotating wing with different Ro, Lentink and Dickinson [10] found that the LEV could be stabilized at low Ro by centripetal and Coriolis accelerations, which mediates the spanwise flow by the effect of 'Ekman pumping' of the boundary layer flow. In the numerical study of Wu *et al* [11] on FWR, a strong spanwise flow on the wing was observed, and the LEV on the FWR wing merged with the tip vortex and the trailing edge vortex (TEV), forming a vortex ring structure that stayed attached on the wing throughout the flapping cycle. These findings suggest that the quasi-steady model is applicable for modelling the aerodynamic forces of FWR and other wing motions in low Ro and low Re flight. It is therefore especially useful for quick estimations of aerodynamic performances for MAVs.

For a particular wing, the quasi-steady coefficients as given in section 2.3 are sensitive to the wing geometry and flow conditions. Lee *et al* [14] numerically investigated the effect of Ro and AR for revolving rectangular wings. They found that both Ro and AR have considerable effect on the vortex dynamics and thus the forces production on the wing. In particular, increasing the AR reduces the three-dimensional tip effect and is thus beneficial to lift generation, while increasing the Ro increases LEV instability, which is detrimental to lift production. In the current study, the quasi-steady coefficients for FWR are obtained by an empirical fit of CFD data for our particular wing geometry, Ro and Re. The results of our model are in good agreement with CFD method in full range of investigations. As shown in Figure 5 and Table 1, compared with CFD, the current model yields maximum differences in lift and rotational moment coefficients of less than 12% and 15%, respectively.

4. Example analysis and results

A unique feature of the FWR is that its rotation is passively induced by the thrust of the flapping wing. This is different from the prescribed motion of insect wings and conventional rotor blades. Consequently, a hovering FWR would reach and stay in an equilibrium rotation speed that the mean aerodynamic thrust balances with the drag of the wing. Thus, the rotational moment would average to zero ($\bar{C}_M = 0$) over a flapping circle. In this study, all the calculations are subjected to the equilibrium state of FWR.

Since the kinematics of FWR is combined by steady rotation and reciprocal flapping motion, a non-dimensional rotation speed η is defined to measure the deflection of the effective AoA:

$$\eta = \frac{\psi_0}{2\Phi f} \qquad (22)$$

where ψ_0 is the rotation speed of the wing in horizontal plane. By equation (20), the mean aerodynamic power coefficient is defined by:

$$\bar{C}_P = \frac{\bar{P}}{0.5\rho U_{\text{ref}}^3 S} \qquad (23)$$

In order to assess the aerodynamic efficiency, the non-dimensional power factor is defined by [10,31,32]:

$$P_f = \frac{\bar{C}_L^{1.5}}{\bar{C}_P} \qquad (24)$$

which measures the power efficiency for sustaining a certain amount of weight for different forms of flight. In the current investigation, P_f is used for the comparison of power efficiency between FWR, RW and insect wings.

Based on the quasi-steady model, the aerodynamic forces and power of FWR under the equilibrium state ($\bar{C}_M = 0$) are calculated at different geometric AoA measured at mid upstrike (α_u) and mid downstroke (α_d). The parameters range between $\alpha_u = 60°\sim0°$ and $\alpha_d = 0°\sim-30°$. In the investigated cases, the flapping amplitude Φ is fixed to $50°$. The flapping frequency and dimension of the wing is determined to match the specified $Re\sim3500$ for the investigation. The resulting non-dimensional parameters of the FWR ($\bar{C}_L$, $\bar{C}_P$, P_f and η) are shown in figure 6.
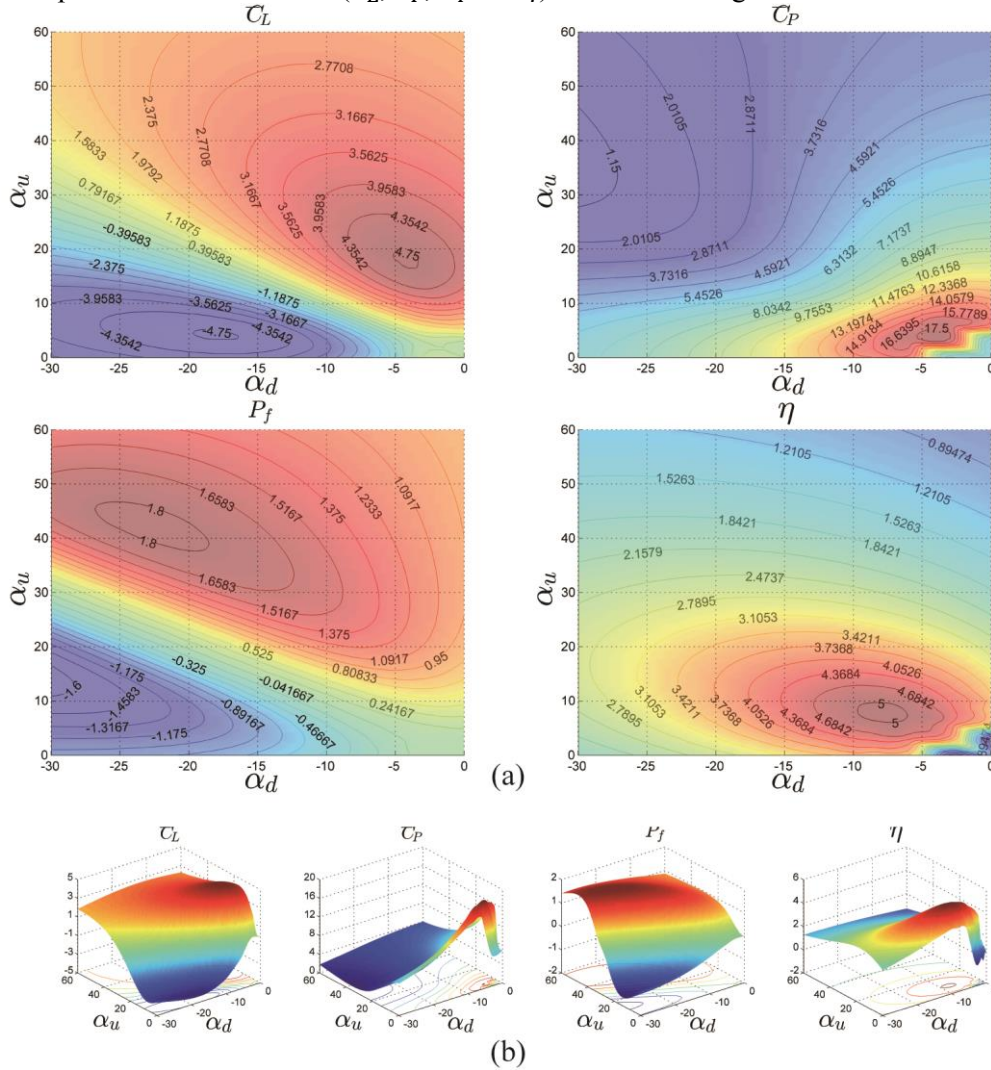
Figure 6. (a) Contour plots and (b) 3D surface plots the FWR results in the range $\alpha_u = 60°\sim0°$ and $\alpha_d = 0°\sim-30°$.

As shown in figure 6, the non-dimensional rotation speed of FWR η is maximized at small anti-symmetric AoA in up and downstroke ($\alpha_u = 9°$ and $\alpha_d = -9°$). Along the symmetry lines $\alpha_d = -\alpha_u$, nearly no lift is generated ($\bar{C}_L\sim0$), thus the power factor P_f remains zero. The power coefficient $\bar{C}_P$ is large at small α_u and α_d where the flapping motion forms large effective AoA. In the special case when the pitch angle is constantly zero ($\alpha_u = \alpha_d = 0$), Vandenberghe et al [33] showed in experiment that the rotation of the wing exhibits supercritical bifurcation, where an inverted von Kármán wake

behind the wing was observed and the wing rotates by the associated thrust. This phenomenon cannot be modelled by the current quasi-steady model.

The results show that the FWR produces high lift coefficient ($\bar{C}_L > 4.3$) when α_d is between $-8°\sim-2°$ and α_u between $13°\sim24°$. The power factor P_f is above 1.6 when $\alpha_d = -30°\sim-13°$ and $\alpha_u = 35°\sim50°$. The resulting maximum values of $\bar{C}_L, P_f, \bar{C}_P$ and η and the associated α_u and α_d are listed in Table 2.

Table 2. The maximum $\overline{C}_L, P_f, \overline{C}_P$ and η values and the associated α_u and α_d.

Dimensionless Parameters	Maximum Values	Equilibrium η at Maximum Values	α_u at Maximum Values	α_d at Maximum Values
$\overline{C}_L$	4.73	3.33	18°	-3°
P_f	1.82	1.94	42°	-24°
$\overline{C}_P$	17.21	4.40	6°	-3°
η	5.03	5.03	9°	-9°

For FWR, the passive rotation speed would deflect the air velocity with respect to the wing which changes the instantaneous effective AoA (α_e, shown in figure 4). Based on the results obtained from figure 6, the instantaneous α_e of the FWR wing at different η are shown in figure 7(a). As can be seen, the variations of α_e in a flapping cycle follow a similar trend for different η. In the downstroke, the wing forms large α_e thus produces large lift and propelling moment. In upstroke, the wing forms small positive α_e thus generates a positive though small lift and anti-rotating moment. Subject to the equilibrium condition ($\bar{C}_M = 0$), the propelling and anti-rotating moments cancel each other over a flapping cycle. The resulting AoAs and forces on the FWR wing are illustrated in figure 7(b).

From figure 7(a), the downstroke α_e changes significantly with the rotation speed (η): a large rotation speed (such as $\eta = 2.70$) produces a small α_e in the downstroke, whereas a small rotation speed ($\eta = 0.99$) results in large α_e in the downstroke. In the former case, the variation of α_e in a flapping cycle appears to be plateaued by the induced rotation speed, thus the aerodynamic force of FWR tends to be dominated by rotation, which is similar to a rotary wing. For the latter case, the wing forms large α_e in the downstroke, whereas a small α_e in the upstroke. The resulting kinematics is similar to a typical insect wing with inclined stroke plane.
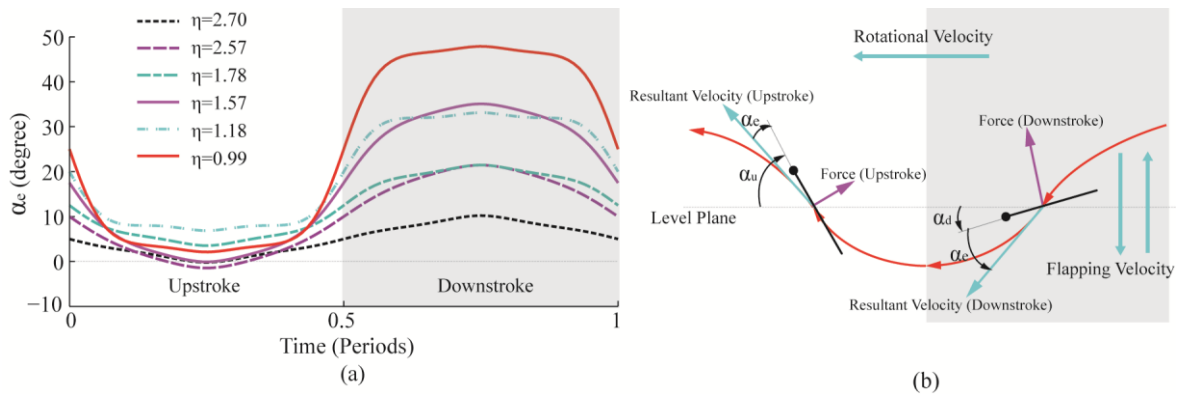

Figure 7. (a) The FWR effective AoA, α_e in different rotation speed and (b) the corresponding velocity and aerodynamic forces.

5. Aerodynamic force and efficiency comparison of three types of wings

5.1. Instantaneous force comparison of FWR with insect-like flapping wings

In order to study the lift production and flight efficiency of the existing types of wing motions (FWR, insect-HF, IF and rotary wing-RW), comparisons are made between these wing kinematics using the same wing geometry (see figure 3) and Re (~3500). The definition of Re for different wings is in the same way with FWR by equation (10). However, for the steady rotation of RW, Re is defined in the usual sense ($Re = \frac{U_t \bar{c}}{\nu}$, where U_t is the wingtip velocity). Similarly, the reference velocity U_{ref} for obtaining the forces coefficients of different wings is chosen as the velocity at R_2 (see equation 21). For the steady rotation of RW, this velocity is given by $U_{ref} = \dot{\psi} R_2$, where $\dot{\psi}$ is the rotation speed.

We first compare the instantaneous aerodynamic force of FWR with the insect flapping wings (HF and IF). The kinematic parameters of FWR are chosen by four representative cases of $\alpha_u = 30°, 60°$ and $\alpha_d = -10°, -20°$, respectively. For insect wings, the kinematic parameters are chosen based on data obtained from typical insect flight. In particular, the HF wing is given by: flapping amplitude $\Phi_{HF} = 150°$ and $\alpha_e = 35°$ in both up and downstroke [34], while the IF wing is given by: $\Phi_{IF} = 90°$, stroke plane inclination angle $\beta = 40°$, and $\alpha_e = 20°$ and $45°$ in the up and downstroke, respectively [35]. The kinematics for different wing motions are illustrated in figure 8. Figure 9 shows the instantaneous lift and rotational moment coefficients for different wings at Re~3500. The associated mean lift and rotational moment coefficients are given in table 3.
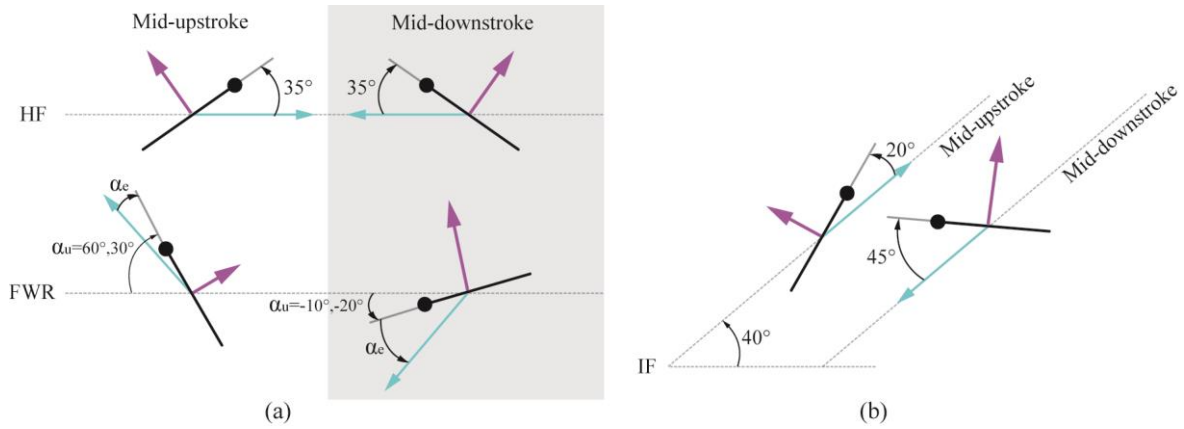
Figure 8. Kinematic for FWR and insect flapping wings. (a)-HF and FWR, (b)-IF.

The instantaneous lift of FWR is similar with the IF, where the downstroke produces the majority of lift while the upstroke contributes small or even negative lift. In contrast, the HF produces equal lift in both up and downstroke. Similar to the IF wing, the large α_e of the FWR wing in the downstroke would produce significant aerodynamic drag (i.e. aerodynamic force parallel to the flow direction). However, a large portion of this drag is contributed to the upward lift due to the vertical flapping velocity. Wang [36] proposed that the aerodynamic drag plays important role for insect flight with an inclined stroke plane: about three quarters of the weight of a dragonfly was supported by the aerodynamic drag. In the above cases of FWR, the drag contribution to the upward lift is between 5%~55%.

For both HF and IF, the wing pitches drastically during a flapping cycle. The typical kinematics of insect wings gives the pitch angles of $\Delta\alpha = 110°$ and $115°$ respectively for HF and IF ($\Delta\alpha$ is defined by the difference of the *Euler* angle α at mid-up and downstroke, see figure 1), whereas the $\Delta\alpha$ of the FWR wing are between $40°$~$80°$. Insect-like flapping wings change the moving direction at stroke reversals, thus the wings need to pitch drastically in order to form a positive α_e in the subsequent stroke. However, due to the induced rotation speed of FWR, a positive α_e can be obtained at a much smaller pitch angle. We anticipate that the smaller pitch angle of the FWR wing would be desirable for MAV structural integrity and actuation system requirements.
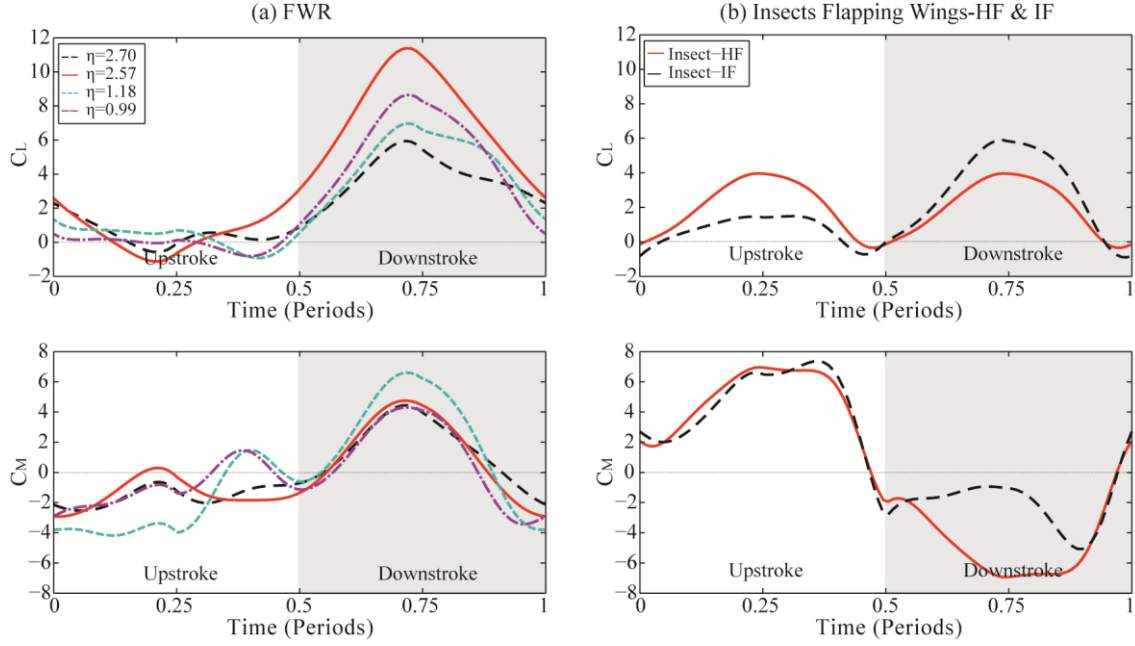
Figure 9. Instantaneous C_L and C_M of FWR and insect flapping wing. (a)-FWR, (b)-HF and IF.

Table 3. Kinematics and corresponding $\bar{C}_L$ and $\bar{C}_M$ of FWR and insect flapping wings (HF and IF).

Kinematic Cases	AoA at mid-upstroke α_u	AoA at mid-downstroke α_d	η	$\bar{C}_L$	$\bar{C}_M$
FWR	30°	-10°	2.57	3.96	0
	30°	-20°	2.70	2.12	0
	60°	-10°	0.99	2.56	0
	60°	-20°	1.18	2.40	0
HF	α_e=35°	α_e=35°	-	1.99	0
IF ($\beta = 40°$)	α_e=20°	α_e=45°	-	1.82	1.20

5.2. Lift and efficiency comparison of three types of wings

The second comparison is between the optimal lift and efficiency of the three types of wings. In this investigation, the kinematic parameters for each wing are specified to vary in a range. The variations of the kinematic parameters are chosen to cover the optimal lift and efficiency for the respective wings. In particular, the α_u and α_d of FWR are chosen to cover the maximum $\bar{C}_L$ and P_f given in table 2; the insect kinematics are chosen to cover the typical motions of insect flight-HF and IF given in table 3. For FWR and IF, the calculations are performed by fixing α_u or α_d respectively in two different cases. The parametric definitions for this investigation are given in table 4 and figure 10.
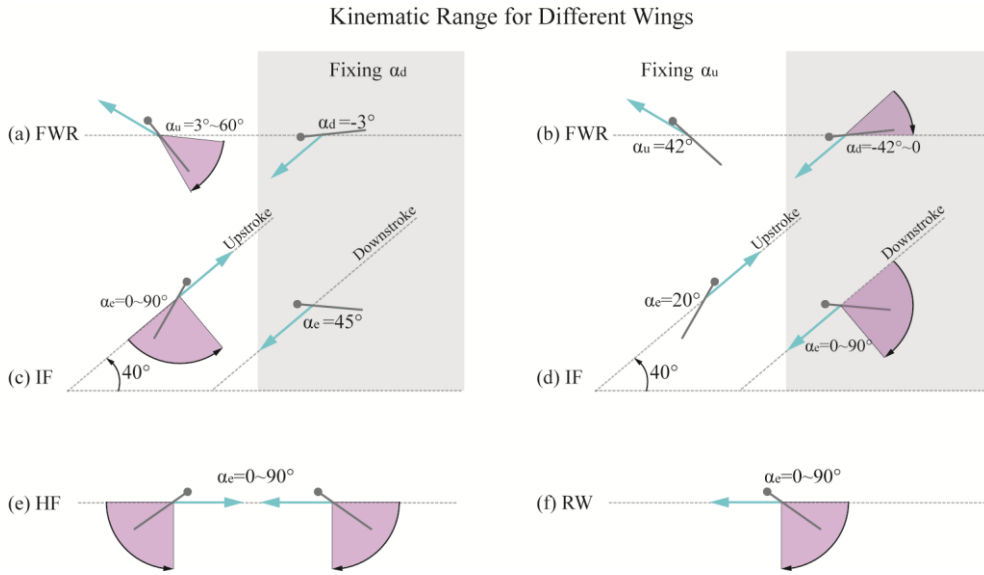
By varying the corresponding parameters (α_u or α_d for FWR and IF, α_e for HF and RW), the chosen parametric spaces thus represent the boundary performances in terms of $\bar{C}_L$ and P_f for the respective wings. The resulting P_f versus $\bar{C}_L$ boundaries for the three types of wings are presented in figure 11. The arrows in the figure indicate the variations of P_f and $\bar{C}_L$ with the increase of the associated AoAs. The typical kinematic case of insect HF is marked by ★, and the dragonfly kinematics case is marked by ▲ (see table 3).

As shown in figure 11, the maximum lift produced by RW is smaller compared with the insect wings (HF and IF) and FWR, but the power factor is greater. This indicates that RW is superior in terms of aerodynamic efficiency among the three types of wings, which is consistent with previous

14

experimental results [10,16]. The maximum P_f of FWR appears to be slightly smaller than RW, but greater than the insect HF and IF wings. This could be due to the deflection of the flow velocity by the passive rotation speed. As shown in figure 7, the rotation speed of FWR tends to plateau the α_e of the wing in both up and downstroke. Therefore, when combined with a suitable flapping amplitude and frequency, the wing of FWR can operate at a relatively constant α_e of high lift to drag ratio, thus produces a higher efficiency, which is similar to the RW operating in a constant AoA.

Table 4. Kinematic parameters and optimal kinematics for three types of wing - FWR, insect-like wings (HF, IF) and RW

| Kinematic Cases		AoA Range-Upstroke	AoA Range-Downstroke	Optimal Kinematics for $\bar{C}_L$ and P_f				
				$\bar{C}_L$	P_f	η	AoA-Up	AoA-Down
FWR	Opt $\bar{C}_L$	α_u=3°~60°	α_d=-3°	4.73	0.98	3.33	α_u=18°	α_d=-3°
	Opt P_f	α_u=42°	α_d=-42°~0°	2.29	1.82	1.94	α_u=42°	α_d=-24°
IF	Opt $\bar{C}_L$	α_e=20°	α_e=0~90°	1.93	0.83	-	α_e=20°	α_e=60°
	Opt P_f	α_e=0~90°	α_e=45°	1.77	0.96	-	α_e=13°	α_e=45°
HF	Opt $\bar{C}_L$	α_e=0~90°		2.04	0.90	-	α_e=42°	
	Opt P_f			1.29	1.56	-	α_e=14°	
RW	Opt $\bar{C}_L$	α_e=0~90°		1.70	1.13	-	α_e=45°	
	Opt P_f			0.72	2.54	-	α_e=12°	

Figure 10. The AoA variation range for (a-b)-FWR, (c-d)-insect IF wing, (e)-insect HF wing and (f)-RW.

It is also noted that the maximum lift of FWR is significantly greater than the other wing motions. This is mainly due to the additional dynamic pressure provided by the passively induced rotation speed. Read *et al* [37] studied the lift and efficiency of a plunging airfoil operating in the free stream. By measuring the fluid forces on the airfoil in a water tank, they found that when the pitching of the airfoil is biased by an angle, significant $\bar{C}_L$ (on the order of 5.5) can be obtained. By using the CFD method, Wang *et al* [38] studied a flapping and simultaneously rotating wing with prescribed rotation speed, when the rotation speed is given by a high value, the obtained $\bar{C}_L$ could be significantly higher,

along with a large anti-rotating moment. Compared with the current investigation of FWR, since the rotation speed of the wing is induced passively by the aerodynamic thrust, the resulting $\bar{C}_L$ is within 5.0 for the specific Re ($\sim 10^3$).

For MAV design, our results show that with the same input motion, i.e. flapping frequency and amplitude, the FWR will produce significant greater lift than the insect flapping wings and also the RW. Therefore, when both vertical lift and aerodynamic efficiency are required for a particular MAV, the FWR type of wing motion would be a suitable candidate for the design choices. In addition, the efficiency to lift boundary given in figure 11 provides a guidance to select the design configuration and suitable kinematic parameters according to the MAV design specifications.
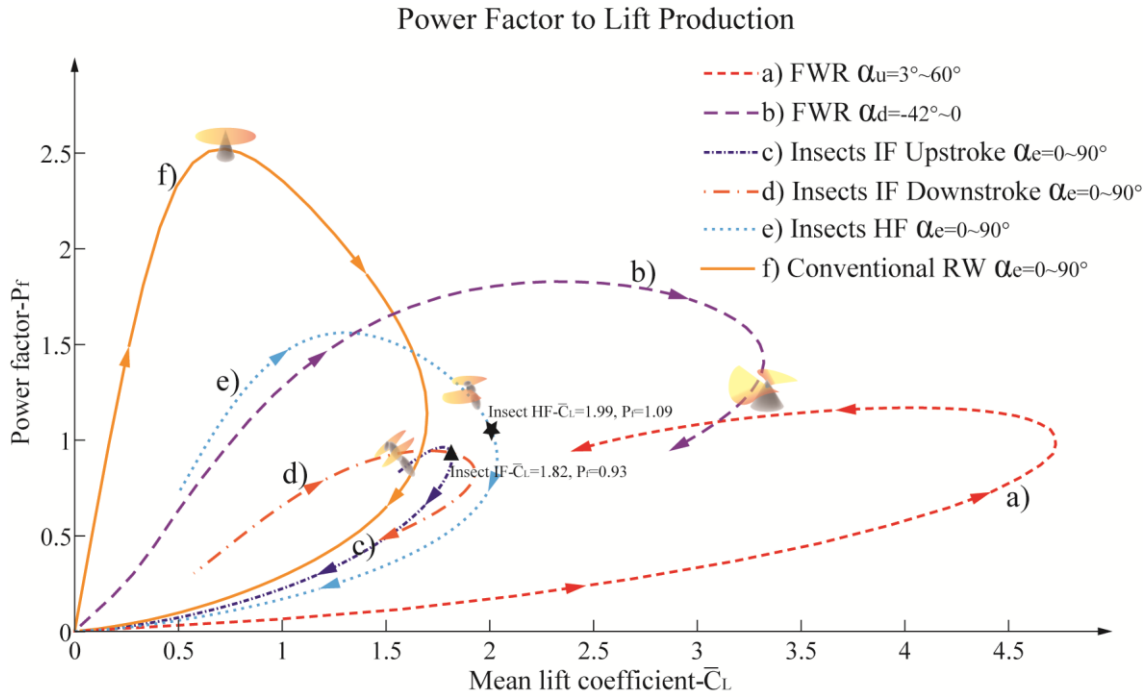
Figure 11. Power factor P_f versus mean lift coefficient $\bar{C}_L$ boundaries for different types of wings.

6. Conclusions

The bioinspired FWR provides a novel MAV configuration by combining the kinematics of motion of rotary and insect-like flapping wings. The FWR rotation is self-propelled in a passive manner by the thrust produced from powered flapping wing motion. This special feature offers not only the capability of VTOLH, but also enhanced aerodynamic performance and simplified mechanical system. A systematic study has been conducted to quantify the FWR performance in terms of aerodynamic lift and power efficiency in a range of kinematic and geometric parameters. The quasi-steady aerodynamic model validated by CFD provides an efficient method of high accuracy for the investigation.

In comparison with the conventional rotary and insect-like flapping wings, the FWR can produce significantly greater aerodynamic lift coefficient with power efficiency between the other two types of wings. The insect-like flapping wings (HF and IF) are of a moderate performance. The rotary wing has the greatest power efficiency of 28% and 39% higher than the FWR and insect-like wing (HF) respectively. However the corresponding lift coefficient of the rotary wing is only 30% and 53% of the other two types of wings respectively. When a rotary wing reaches its maximum lift with compromised power efficiency, the insect wing and FWR can offer 17% and more than double higher lift respectively in the same level of power efficiency. The FWR offers a significantly broader range of

combination of aerodynamic lift and power efficiency with optional kinematics of wing motion. The study results provide a quantified guidance for the three types of wing design option together with the optimal kinematics of motion according to specified MAV flight performance requirements.

References

[1]   D. Lentink, Biomimetics: Flying like a fly, Nature. 498 (2013) 306–307.

[2]   S. Guo, D. Li, Z. Huang, A smart material aeroelastic flapping wing micro rotorcraft, in: Int. Forum Aeroelasticity Struct. Dyn., 2009.

[3]   C.P. Ellington, The Aerodynamics of Hovering Insect Flight .4. Aerodynamic Mechanisms, Philos. Trans. R. Soc. London Ser. B-Biological Sci. 305 (1984) 79-. doi:10.1098/rstb.1984.0052.

[4]   M.H. Dickinson, F.O. Lehmann, S.P. Sane, Wing rotation and the aerodynamic basis of insect flight, Science (80-.). 284 (1999) 1954–1960. doi:10.1126/science.284.5422.1954.

[5]   C.P. Ellington, C. van den Berg, A.P. Willmott, A.L.R. Thomas, Leading-edge vortices in insect flight, Nature. 384 (1996) 626–630. doi:10.1038/384626a0.

[6]   H. Lu, K.B. Lua, Y.J. Lee, T.T. Lim, K.S. Yeo, Ground effect on the aerodynamics of three-dimensional hovering wings., Bioinspir. Biomim. 11 (2016) 66003. doi:10.1088/1748-3190/11/5/066003.

[7]   K.B. Lua, Y.J. Lee, T.T. Lim, K.S. Yeo, Aerodynamic Effects of Elevating Motion on Hovering Rigid Hawkmothlike Wings, AIAA J. 54 (2016) 1–18. doi:10.2514/1.J054326.

[8]   M.H. Dickinson, K. Götz, Unsteady aerodynamic performance of model wings at low reynolds numbers, J. Exp. Biol. 174 (1993) 45–64. doi:10.1242/jeb.00739.

[9]   T.T. LIM, C.J. TEO, K.B. LUA, K.S. YEO, ON THE PROLONG ATTACHMENT OF LEADING EDGE VORTEX ON A FLAPPING WING, Mod. Phys. Lett. B. 23 (2009) 357–360. doi:10.1142/S0217984909018394.

[10]   D. Lentink, M.H. Dickinson, Rotational accelerations stabilize leading edge vortices on revolving fly wings, J. Exp. Biol. 212 (2009) 2705–2719. doi:10.1242/jeb.022269.

[11]   J. Wu, D. Wang, Y. Zhang, Aerodynamic Analysis of a Flapping Rotary Wing at a Low Reynolds Number, AIAA J. 53 (2015) 2951–2966. doi:10.2514/1.J053845.

[12]   C. Zhou, J. Wu, S. Guo, D. Li, Experimental study on the lift generated by a flapping rotary wing applied in a micro air vehicle, Proc. Inst. Mech. Eng. Part G-J. Aerosp. Eng. 228 (2014) 2083–2093. doi:10.1177/0954410013512761.

[13]   S. Guo, D. Li, J. Wu, Theoretical and experimental study of a piezoelectric flapping wing rotor for micro aerial vehicle, Aerosp. Sci. Technol. 23 (2012) 429–438. doi:10.1016/j.ast.2011.10.002.

[14]   Y.J. Lee, K.B. Lua, T.T. Lim, Aspect ratio effects on revolving wings with Rossby number consideration., Bioinspir. Biomim. 11 (2016) 56013. doi:10.1088/1748-3190/11/5/056013.

[15]   J.R. Usherwood, C.P. Ellington, The aerodynamics of revolving wings - I. Model hawkmoth wings, J. Exp. Biol. 205 (2002) 1547–1564.

[16]   D. Lentink, S.R. Jongerius, N.L. Bradshaw, The Scalable Design of Flapping Micro-Air Vehicles Inspired by Insect Flight, Fly. Insects Robot. (2009) 185–205. doi:Doi 10.1007/978-3-540-89393-6_14.

[17]   S.P. Sane, M.H. Dickinson, The control of flight force by a flapping wing: Lift and drag production, J. Exp. Biol. 204 (2001) 2607–2626.

[18]   S.P. Sane, M.H. Dickinson, The aerodynamic effects of wing rotation and a revised quasi-

steady model of flapping flight, J. Exp. Biol. 205 (2002) 1087–1096.

[19]   Z.J. Wang, J.M. Birch, M.H. Dickinson, Unsteady forces and flows in low Reynolds number hovering flight: two-dimensional computations vs robotic wing experiments, J. Exp. Biol. 207 (2004) 449–460. doi:10.1242/jeb.00739.

[20]   J.H. Wu, M. Sun, Unsteady aerodynamic forces of a flapping wing, J. Exp. Biol. 207 (2004) 1137–1150. doi:10.1242/jeb.00868.

[21]   C.P. Ellington, The Aerodynamics of Hovering Insect Flight .2. Morphological Parameters, Philos. Trans. R. Soc. London Ser. B-Biological Sci. 305 (1984) 17–40. doi:10.1098/rstb.1984.0050.

[22]   M. Sun, J.H. Wu, Aerodynamic force generation and power requirements in forward flight in a fruit fly with modeled wing motion, J. Exp. Biol. 206 (2003) 3065–3083. doi:10.1242/jeb.00517.

[23]   J.P. Whitney, R.J. Wood, Aeromechanics of passive rotation in flapping flight, J. Fluid Mech. 660 (2010) 197–220. doi:10.1017/S002211201000265X.

[24]   L.I. Sedov, Two-dimensional problems of hydrodynamics and aerodynamics, Moscow Izd. Nauk. 1 (1980).

[25]   Y.J. Lee, K.B. Lua, T.T. Lim, K.S. Yeo, A quasi-steady aerodynamic model for flapping flight with improved adaptability, Bioinspir. Biomim. 11 (2016) 36005. doi:10.1088/1748-3190/11/3/036005.

[26]   a. Andersen, U. Pesavento, Z.J. Wang, Unsteady aerodynamics of fluttering and tumbling plates, J. Fluid Mech. 541 (2005) 65. doi:10.1017/S002211200500594X.

[27]   W.B. Dickson, A.D. Straw, C. Poelma, M.H. Dickinson, An integrative model of insect flight control, in: Proc. 44th AIAA Aerosp. Sci. Meet. Exhib., 2006: pp. 31–38. doi:10.2514/6.2006-34.

[28]   M.H. Dickinson, J.R.B. Lighton, Muscle Efficiency and Elastic Storage in the Flight Motor of Drosophila, Science (80-.). 268 (1995) 87–90. doi:10.1126/science.7701346.

[29]   G.J. Berman, Z.J. Wang, Energy-minimizing kinematics in hovering insect flight, J. Fluid Mech. 582 (2007) 153–168. doi:10.1017/S0022112007006209.

[30]   K.B. Lua, T.T. Lim, K.S. Yeo, Scaling of Aerodynamic Forces of Three-Dimensional Flapping Wings, AIAA J. 52 (2014) 1–7. doi:10.2514/1.J052730.

[31]   Z.J. Wang, Aerodynamic efficiency of flapping flight: analysis of a two-stroke model, J. Exp. Biol. 211 (2008) 234–238. doi:10.1242/jeb.013797.

[32]   G.J.J. Ruijgrok, Elements of airplane performance, Delft university press, 1990.

[33]   N. Vandenberghe, J. Zhang, S. Childress, Symmetry breaking leads to forward flapping flight, J. Fluid Mech. 506 (2004) 147–155. doi:10.1017/S0022112004008468.

[34]   C.P. Ellington, The Aerodynamics of Hovering Insect Flight .3. Kinematics, Philos. Trans. R. Soc. London Ser. B-Biological Sci. 305 (1984) 41-. doi:10.1098/rstb.1984.0051.

[35]   A. Azuma, S. Azuma, I. Watanabe, T. Furuta, Flight Mechanics of a Dragonfly, J. Exp. Biol. 116 (1985) 79–107. http://jeb.biologists.org/content/116/1/79.abstract.

[36]   Z.J. Wang, The role of drag in insect hovering, J. Exp. Biol. 207 (2004) 4147–4155. doi:207/23/4147 [pii].

[37]   D.A. Read, F.S. Hover, M.S. Triantafyllou, Forces on oscillating foils for propulsion and maneuvering, J. Fluids Struct. 17 (2003) 163–183. doi:10.1016/S0889-9746(02)00115-9.

[38]   D. Wang, Y. Zhang, J. Wu, Y. Zhang, Aerodynamics on Flapping Rotary Wing in Low Reynolds Number, (2013) 1–14. doi:10.2514/6.2013-4382.